OPERATION AND PERFORMANCE OF THE HIGH-INTENSITY
PROTON INJECTOR OF LAMPF*

by

D. W. Mueller, E. A. Meyer, R. R. Stevens, Jr.,
B. C. Goplen, MP-9, M. A. Paciotti, MP-3
and C. R. Emigh, P-DOR

Los Alamos Scientific Laboratory
of the University of California
Los Alamos, New Mexico

ABSTRACT

The recent operational experience with the LAMPF high-intensity
proton injector is presented. Extensive beam measurements have been
carried out on the ion beam extracted from the accelerating column
and the results are compared with the behavior expected from a Pierce
column. Improvements made in the ion source and other injector sys-
tems are presented; operation over a wider range of extracted currents
without arc down is now possible. A major cause of arc down in the
accelerating column was traced to occasional failure of the arc modu-
lator turn-off circuit and has been eliminated. A procedure for en-
hancing the hydrogen pumping speed of the ion pumps is discussed.

I. INTRODUCTION

The high-intensity proton injector for LAMPF
has been in operation for over two years and has
been used to supply 750-kV proton beams for the ini-
tial testing and preliminary operation of the LAMPF
accelerator. Most of the operating problems pre-
viously reported[1] have been corrected, and the in-
jector is now quite reliable at low-duty factor
operation. During the initial 800-MeV turn on of
LAMPF, this injector ran for 92 h with only one arc
down. Work is still in progress to improve the arc-
down rate at high-duty factor operation.

Difficulties experienced in optimizing the per-
formance of the injector beam transport system led
to a series of beam measurements at the exit of the
accelerating column. The transverse emittance of
extracted beam was measured for a wide range of ion
source parameters and the properties of the beam en-
tering the transport line were experimentally deter-
mined. Using these results, a new design for this
transport system was calculated and subsequently
implemented.

II. COCKCROFT-WALTON HIGH-VOLTAGE GENERATOR

Modifications have been made to improve the
performance of the Cockcroft-Walton (C-W) bouncer
circuits. The loop gain available to drive the
series FHT7 was increased in order to improve the
dynamic response of this system. It was then nec-
essary to introduce additional current feedback
since the control loop was almost unstable. The
initial voltage drop in the bouncer is now ~ 250 V
for a 40-mA current pulse, and after the first 10
μsec the variation in voltage is about ± 75 V or
± 0.01% of the 750-kV operating voltage.

III. DUOPLASMATRON ION SOURCE

During the past year the duoplasmatron ion
source has been in operation for over 3000 h with
the new design for the anode aperture plate shown
in Fig. 1. The only component failure in this
source during this time has been a filament which
was severed after 2000 h of operation. Some erosion
of the anode aperture was noted at this time; the
aperture had increased from 0.025- to 0.031-in. diam

and was slightly elliptical. During the first six
months of operation with the new anode aperture, the
proton fraction from the source slowly decreased
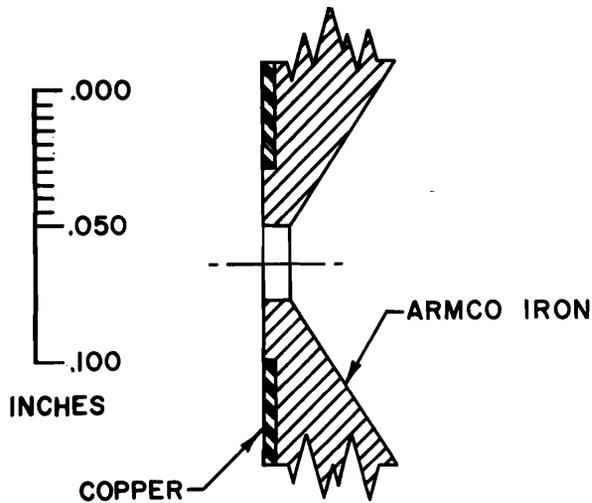from 82 to 70% but now appears to have stabilized.

Fig. 1. Anode aperture plate for the LAMPF duo-
plasmatron.

Fig. 2. Magnetic field measurements in the expan-
sion cup of the LAMPF duoplasmatron. The
variation of magnetic field along the duo-
plasmatron axis and the variation of the
magnetic field with magnet current at a
point 0.25 in. downstream from the Pierce
anode are shown.

The source has been modified to provide hydro-
gen gas feed lines and pressure monitors through
the side wall of the source into the space between
the plasma anode aperture and the intermediate elec-
trode. No change in operation of the source was
noted, contrary to our expectations. The use of
side feed lines does permit easier replacement of
the filament and arc magnet coil.

Work has been recently carried out to measure
the magnetic field in the expansion cup region of
duoplasmatron in order to understand changes in beam
size observed with arc magnet current. The magnetic
field observed is shown in Fig. 2.

IV. COLUMN ARC-DOWN STUDIES

A major cause of column arc-down under low-
power operating conditions was traced to a malfunc-
tion of the modulator controlling the ion source.
Turning on the beam after it had been off for more
than 8 sec invariably caused an arc-down.

The problem was caused by the decay of a delay
line voltage which occurred when the input signals
to the modulator were turned off. This condition
left insufficient voltage for the SCR to turn off
the beam at the end of the beam gate pulse and re-
sulted in a long pulse with beam current gradually
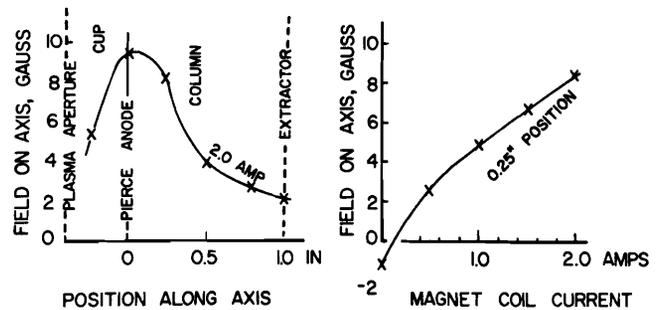decreasing to zero over 5000 μsec as the modulator

capacitor discharged. With the extractor voltage
set for the design current level, the diminishing
beam current would inevitably spray the electrodes.
Apparently some delay mechanism is involved since
the actual arc-down always occurred about 20 msec
after the end of the long pulse. Installation of
a simple charging circuit to keep sufficient vol-
tage on the delay line at all times has eliminated
this problem.

Observations to date show essentially all other
arc-downs at 60 and 120 Hz are beam induced, occur-
ring during the beam pulse or shortly thereafter.
At very low repetition rates (e.g., 3.75 Hz) arc-
downs are rare, and a much smaller percentage is
beam-induced.

The accelerating column has remained on-line
since it was installed. All repairs and modifica-
tions have been made on-line through the access
ports in the transparent acrylic jacket.

V. ACCELERATING COLUMN TESTS

An extensiv. series of beam measurements has
been carried out to determine the properties of the
beam extracted from the accelerating column. These
studies were motivated by the desire to do more real-
istic calculations for the injector beam transport
system. A series of 104 high resolution, pepper-pot

emittance photographs was taken with a titanium pepper-pot assembly shown in Fig. 3. The layout for these experiments is presented in Fig. 4 and a typical emittance pattern photograph is shown in Fig. 5.
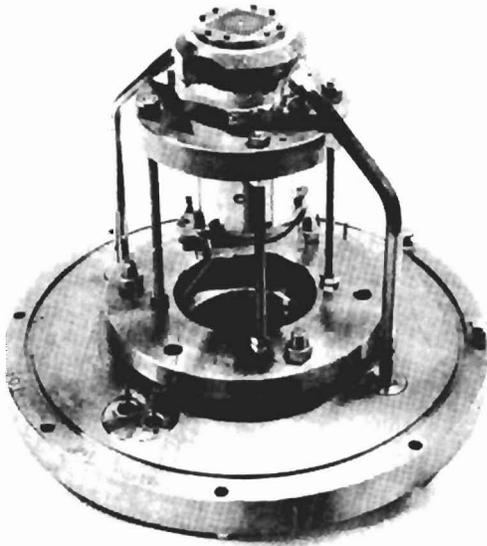

Fig. 3. Pepper-pot emittance measuring device used in the accelerating column beam tests.

Fig. 4. Layout of the components employed in the accelerating column beam tests.

Electron neutralization effects were neglected because the pepper pot was biased to a sufficient voltage to prevent secondary electrons from escaping. Moreover, the gas pressure in the accelerating tube was sufficiently low ($\sim 1 \times 10^{-5}$) to preclude any
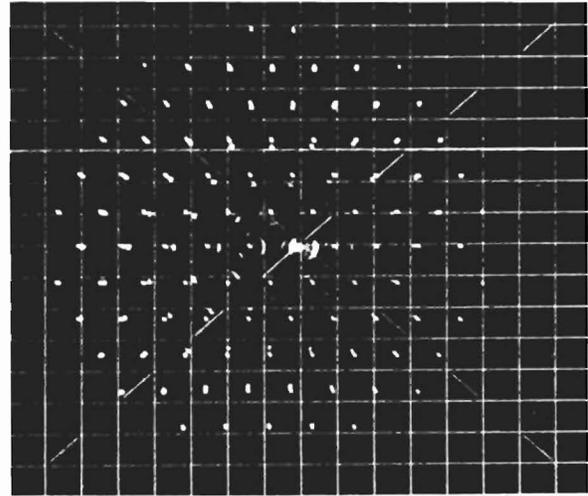

Fig. 5. Pepper-pot emittance pattern for a 50-mA extracted beam at 1.75 A magnet current.

significant neutralization from gas ionization. The data on these photographs were digitized and analyzed by a computer data reduction process. The envelope size and divergence of the exit beam were determined in each case and a graph showing these results is presented in Fig. 6; a tabulation of beam parameters is presented in Table I. When the accelerating column was operated at the emittance corrected Pierce current[†] (45.3 mA for a 70% proton
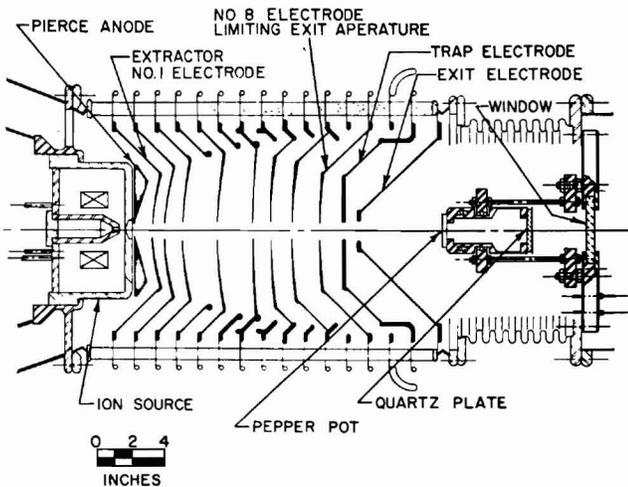

Fig. 6. Summary of pepper-pot data showing envelope size and divergence of the beams observed.

TABLE I

Picture No.	Arc Magnet Current (A)	Extractor Voltage (V)	Electron Trap Voltage (kV)	Transformer Current (mA)	Chamber Pressure (μ)	Repetition Rate (Sec⁻¹)	Pulse Width (μsec)
1A	1.75	25.8	-10	48	98	15	100
2A	1.75	25.8	-10	48	98	15	100
3A	1.75	27.0	-10	48	98	15	100
4A	2.37	25.8	-10	48	98	15	100
5A	1.75	25.8	-10	32	98	15	100
6A							
7A	1.75	25.8	-10	44	98	15	100
8A	1.75	25.8	-10	49	98	15	100
9A	1.75	25.8	-10	50	98	15	100
10A	1.75	25.8	-10	36	98	15	100
1B	1.75	25.8	-10	10	120	15	100
2B	1.75	25.8	-10	20	120	15	100
3B	1.75	25.8	-10	28	120	15	100
4B	1.75	25.8	-10	32	120	15	100
5B	1.75	25.8	-10	36	120	15	100
6B	1.75	25.8	-10	40	120	15	100
1	1.75	25.8	-10	10	120	15	100
2	1.75	25.8	-10	20	120	15	100
3	1.75	25.8	-10	28	120	15	100
4	1.75	25.8	-10	32	120	15	100
5	1.75	25.8	-10	36	120	15	100
6	1.75	25.8	-10	40	120	15	100
7	1.75	25.8	-10	44	120	15	100
8	1.75	25.8	-10	48	120	15	100
9	1.75	27.0	-10	48	120	15	100
10	1.75	27.0	-10	44	120	15	100
11	1.75	27.0	-10	40	120	15	100
12	1.75	27.0	-10	36	120	15	100
13	1.75	27.0	-10	32	120	15	100
14	1.75	27.0	-10	28	120	15	100
15	1.75	27.0	-10	20	120	15	100
16	1.75	27.0	-10	10	120	15	100
17	2.50	25.8	-10	10	120	15	100
18	2.6	25.8	-10	7	120	15	100
19	1.7	25.8	-10	10	120	15	100
20	2.6	25.8	-10	10	120	15	100
21	2.6	25.8	-10	20	120	15	100
22	2.6	25.8	-10	28	120	15	100
23	2.6	25.8	-10	32	120	15	100
24	2.6	25.8	-10	36	120	15	100
25	2.60	25.8	-10	40	120	15	100
26	2.60	25.8	-10	44	120	15	100
27	2.60	25.8	-10	48	120	15	100
28	2.54	27.0	-10	48	120	15	100
29	2.54	27.0	-10	44	120	15	100
30	2.54	27.0	-10	40	110	15	100
31	2.54	27.0	-10	36	110	15	100
32	2.54	27.0	-10	32	110	15	100
33	2.54	27.0	-10	28	110	15	100
34	2.54	27.0	-10	20	110	15	100
35	2.54	27.0	-10	10	110	15	100
36	1.75	27.0	-10	48	120	15	100
37	1.75	27.0	-10	48	120	15	100
38	1.75	27.0	-10	48	120	15	100
39	1.75	27.0	-10	48	120	15	100
40	1.75	27.0	-10	48	130	15	100
41	1.75	27.0	-10	48	130	15	100
42	1.75	27.0	-10	48	140	15	100
43	2.54	27.0	-10	10	110	15	100

TABLE I
(continued)

Picture No.	Arc Magnet Current (A)	Extractor Voltage (V)	Electron Trap Voltage (kV)	Transformer Current (mA)	Chamber Pressure (μ)	Repetition Rate (Sec^{-1})	Pulse Width (μsec)
44	1.75	25.8	-10	10	110	120	10
45	1.75	25.8	-10	20	110	120	10
46	1.75	25.8	-10	28	110	120	10
47	1.75	25.8	-10	32	135	120	10
48	1.75	25.8	-10	36	135	120	10
49	1.75	25.8	-10	40	135	120	10
50	1.75	25.8	-10	44	135	120	10
51	1.75	25.8	-10	38	135	120	10
52	1.75	25.8	-10	51	135	120	10
53	1.75	25.8	-10	10	100	120	20
54	1.75	25.8	-10	20	100	120	10
55	1.75	25.8	-10	28	100	120	10
56	1.75	25.8	-10	32	100	120	10
57	1.75	25.8	-10	36	100	120	10
58	1.75	25.8	-10	40	105	120	10
59	1.75	25.8	-10	44	110	120	20
60	1.75	25.8	-10	48	140	120	20
61	1.75	25.8	-10	50	140	120	20
62	1.75	25.8	-10	10	170	15	100
63	1.75	25.8	-10	20	170	15	100
64	1.75	25.8	-10	28	170	15	100
65	1.75	25.8	-10	32	170	15	100
66	1.75	25.8	-10	36	170	15	100
67	1.75	25.8	-10	40	170	15	100
68	1.75	25.8	-10	44	170	15	100
69	1.75	25.8	-10	48	170	15	100
70	1.75	25.8	-10	50.5	170	15	100
71	1.75	25.8	- 5	10	125	15	100
72	1.75	25.8	- 5	20	125	15	100
73	1.75	25.8	- 5	28	125	15	100
74	1.75	25.8	- 5	32	125	15	100
75	1.75	25.8	- 5	36	125	15	100
76	1.75	25.8	- 5	40	125	15	100
77	1.75	25.8	- 5	44	125	15	100
78	1.75	25.8	- 5	48	130	15	100
79	2.60	25.8	- 5	48	130	15	100
80	2.60	25.8	- 5	44	130	15	100
81	2.60	25.8	-10	44	130	15	100
82	2.60	25.8	- 5	30	130	15	100
83	1.75	25.8	-10	44	130	15	100
84							
85	1.75	27.0	0	32	65	15	100
86	1.75	27.0	0	40	65	15	100
87	1.75	27.0	0	48	80		
88	1.75	27.0	-10	40	80	15	100

fraction), the observed beam size and envelope divergence at the pepper pot was 1.2-cm radium and 15.1 mrad respectively.

To allow comparison with previous estimates of the beam phase space, the data of Fig. 6 were transformed back to the center plane of the tenth electrode. This procedure allows beam transport calculations to be done from the exit of the column. The transformation was done with an azimuthally symmetric Kapchinskij-Vladimirskij envelope code. Consideration was taken of the higher charge density of the H_2^+ ion species. The results obtained after this transformation for beams with various beam currents at the standard operating conditions are presented in Fig. 7. In particular, for the case where the accelerating column was operated at the emittance corrected Pierce current (45.3 mA), a beam size of 1.0-cm radius and an envelope divergence of 14.6 mrad was obtained at the exit of the accelerating column. For this beam size, the exit lens effect of the accelerating column will account for 11.0 mrad of envelope divergence. The remainder of the envelope divergence and the growth of the beam size in the accelerating tube itself is believed to be due to the details of the phase space distribution of the beam extracted from the plasma surface in the duoplasmatron.
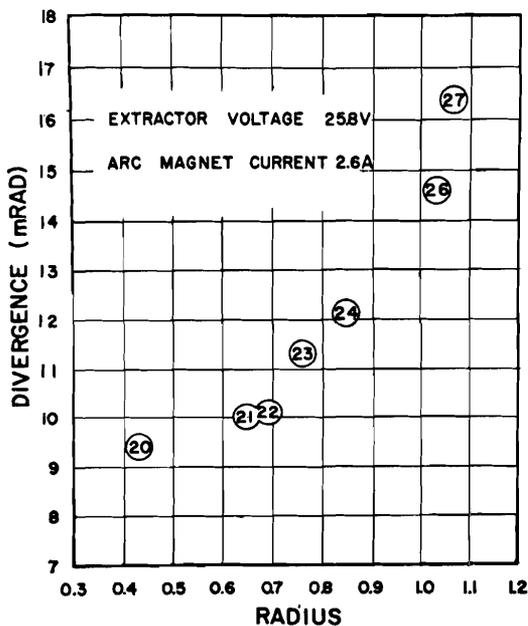

Fig. 7. Pepper-pot data showing envelope size and divergence at the exit of the accelerating column for beams run at standard operating conditions.

VI. COLUMN OPERATION - OFF DESIGN CURRENTS

The Pierce electrodes in the accelerating tube (see Fig. 4) were initially designed to compensate for the space charge of a 50-mA proton beam. The voltage gradient of the tube was subsequently changed by the addition of an electron trap biased at -10 kV, changing the design current of the tube to 55.6 mA of protons. For a typical $H^+/H_2^+/H_3^+$ species ratio of 70/25/5, the column current required to produce the same space charge loading is 51.8 mA. A further correction has been made to take into account the finite emittance of the beam extracted from the ion source; this correction consists in reducing the extractor voltage and the extracted current from the Pierce design value in order to obtain some|focusing after the extractor. The basis of this correction was a theoretical estimate of the conditions required to keep the rms radius of the beam constant in the column. The emittance-corrected Pierce current (ECPC) is 45.3 mA which corresponds to an extractor voltage of 25.8 kV, assuming a beam emittance of 1.25 π-cm mrad at 750 kV. These conditions are then the emittance-corrected design conditions for this accelerating column.

During the first 2 years of operation the current extracted from the accelerating column was often chosen at a value different from the design current while keeping the extractor voltage constant at the emittance-corrected design value (25.8 kV). At currents appreciably above and below the emittance corrected Pierce current (ECPC) the beam was scraped on the column electrodes and the x-ray background from the column increased as shown in Fig. 8. At current well below the ECPC, the tails (crossover satellite structures) of the beam are being scraped on the column electrodes while for current somewhat above ECPC, the space charge blowup of the beam is causing the main core of the beam to be scraped by the electrodes.

In order to achieve optimal operation of the accelerating column and to minimize aberrations in the beam, it is desirable to operate the duoplasmatron so that the ion beam is extracted from a nearly flat plasma surface. Thus, as the operating parameters of the ion source are varied to obtain other extracted currents than ECPC, the extractor voltage should be varied to keep the plasma surface flat.
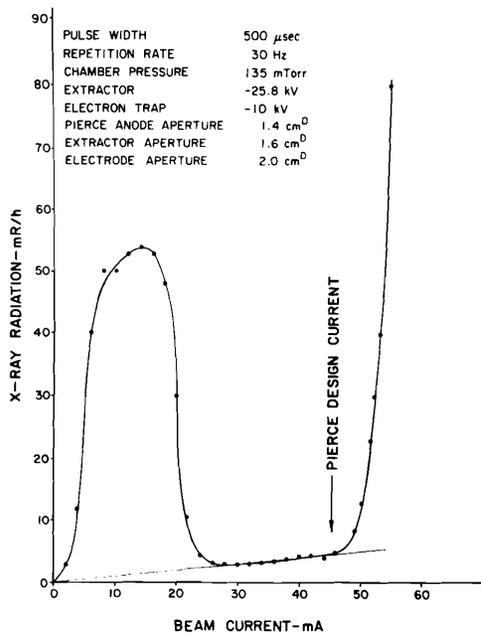
383

Fig. 8. Measured x-ray radiation at the door of the C-W Faraday cage as a function of extracted current from the accelerating column. The extractor voltage is held constant at the value determined by the Child-Langmuir law for the design current (ECPC) of the accelerating column.
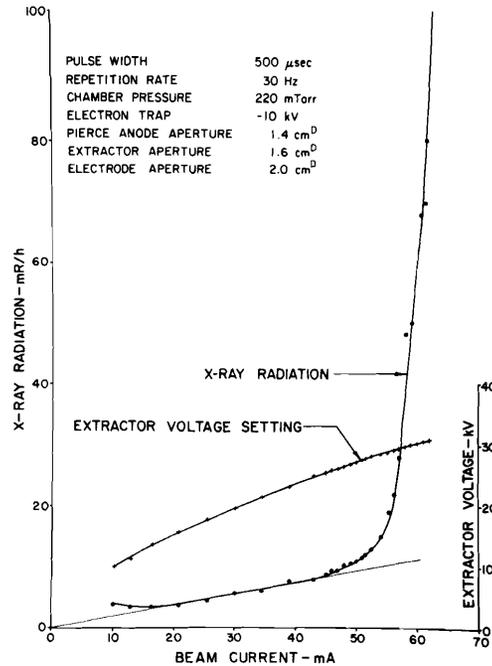

Fig. 9. Measured x-ray radiation at the door of the C-W Faraday cage as a function of extracted current from the accelerating column. For each extracted current, the extractor voltage was adjusted in accordance with the Child-Langmuir law. The extractor voltage is also plotted.

The required voltage variation is determined by the Child-Langmuir Law:

$$V = 6.959 \times 10^4 \left(\frac{I_p}{\pi R^2}\right)^{2/3} z^{4/3} \text{ volts}$$

where R is the beam radius in cm, z is the distance along the column axis in cm. I_p is the equivalent proton current in amperes, given by:

$$I_p = I\alpha = I\left(\frac{H_1^+}{\sum\limits_{i=1}^{3} H_i^+} + \frac{H_2^+ \sqrt{2}}{\sum\limits_{i=1}^{3} H_i^+} + \frac{H_3^+ \sqrt{3}}{\sum\limits_{i=1}^{3} H_i^+}\right)$$

where I is the measured current extracted and the fractions are the indicated species ratio.

Programming the extractor voltage in accordance with the extracted current in this manner keeps the plasma surface nearly flat and thus moves the ion optic lens from the plasma surface to the extractor region. As the extractor voltage is lowered, additional focusing then occurs at the extractor electrode. As a result, x-ray radiation has been almost eliminated at the lower currents (Fig. 9) and the onset of high radiation production has been extended to higher peak currents.

The shape of the x-ray radiation curve in the 20- to 50-mA range is significant. The measured radiation is linear with current and the extrapolated curve passes through the origin. This radiation is attributed to backstreaming electrons from ionization of the residual gases in the accelerating tube. This ionization, and hence the radiation, should be proportional to beam current and gas pressure. Any deviation of radiation from linearity would then indicate that the beam is being scraped by the electrodes. This hypothesis has been confirmed by measuring the current to the electrodes and changing the gas pressure in the column. It is important to note that this low radiation level would be completely masked if it were not for the electron trap which prevents backstreaming electrons from entering the accelerating tube.

The effectiveness of the electron trap is illustrated in Fig. 10 which shows the x-ray background as a function of electron trap voltage.

To test the concept of radiation resulting from residual gas ionization, the hydrogen pressure in the accelerating tube was reduced from 3.9×10^{-5} to 1.5×10^{-5} torr, resulting in a corresponding

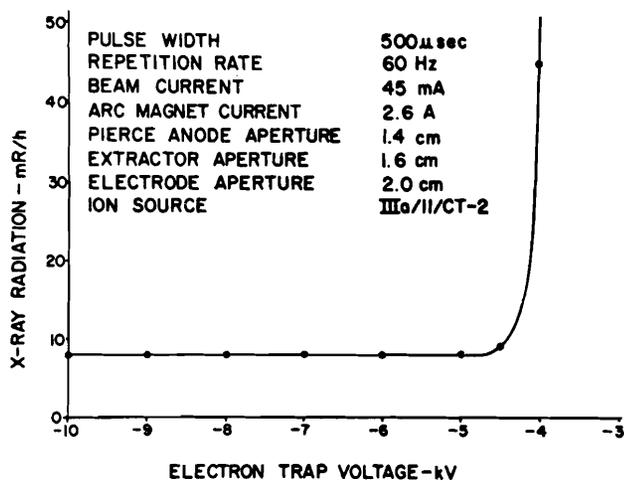| PULSE WIDTH | 500μsec |
REPETITION RATE	60 Hz
BEAM CURRENT	45 mA
ARC MAGNET CURRENT	2.6 A
PIERCE ANODE APERTURE	1.4 cm
EXTRACTOR APERTURE	1.6 cm
ELECTRODE APERTURE	2.0 cm
ION SOURCE	IIIa/II/CT-2

Fig. 10. X-ray background radiation as a function of electron trap voltage.

decrease in radiation from 10 to 6 mR/h at the outside wall of the Faraday cage. Using the radiation yield as an indication of beam impingement on the electrodes, it must be concluded that no significant amount of current strikes the electrodes between 20 mA and the emittance-corrected Pierce current (45.3 mA). Since we have observed a direct relationship between radiation level and column arc downs, programming the extractor voltage will result in more reliable operation with fewer arc downs from being impingement on the electrodes.

VII. ENHANCED HYDROGEN PUMPING

During the accelerating column beam tests, frequent opening of the vacuum system caused an appreciable time loss waiting for the hydrogen ion pump to achieve enhanced pumping. The problem may have been aggravated by having only one pump in service which was almost ready for replacement.

The loss in pumping speed after opening the system is due to nitrogen creating a surface barrier to the diffusion of molecular hydrogen into the titanium as discussed by Singleton.[2,3] When this surface barrier is present, only ionized hydrogen can be pumped. If the surface barrier is removed, both hydrogen ions and molecular hydrogen are pumped and the total pumping speed is about 2-1/2 times the ionic component alone. The ionic pumping speed of each of our hydrogen ion pumps is about 1200 ℓ/sec and if we remove the surface barrier on the titanium, we can increase this to 3000 ℓ/sec. With two pumps

in parallel, the additional 3600 ℓ/sec available due to enhancement pumping is sufficient incentive to remove this impurity layer and prevent it from reforming during operation. It is essential that all leaks in the vacuum system be eliminated since this barrier on the titanium can be formed by as little as 3×10^{-8} torr partial pressure of nitrogen.

This surface barrier can be removed by sputtering with hydrogen during normal operation but this takes 24 to 48 h. Argon is at least 100 times more efficient than hydrogen and has been used to enhance the pumping of hydrogen in sputter ion pumps.[4] After every pump down, we remove this impurity layer by introducing argon into the system at 2×10^{-5} torr. A 20-min treatment with the pump operating is sufficient to enhance the pumping speed by a factor of 2-1/2. For the same chamber pressure of 80 mtorr of hydrogen, the vacuum system pressure dropped from 1.3×10^{-5} to 5×10^{-6} torr as a result of the argon sputtering. Another advantage of this enhanced mode of pumping is the substantial reserve pumping speed for hydrogen even when power is inadvertently removed from the pump. While the ionic pumping is then reduced to zero, the residual molecular hydrogen and other active gases will still be pumped by the clean titanium surfaces, which will keep the pressure relatively low for days in a clean, tight system.

VIII. BEAM TRANSPORT SYSTEM

A beam transport system is used to transport proton beams from the injector to the first tank of the linac and has been previously reported. Initial operation of this system met design goals but indicated that greater beam currents could be transported to the linac if beam loss at the prebuncher were reduced. As a result of the accelerating column tests, a new design for the transport system was calculated and additional quadrupole lenses were added. The details of the new transport design are discussed in another paper in these proceedings.[†]

Additional viewing screens have added to the beam line so that beam cross sections can now be observed at four points along this beam line. A photo-

---

[†]R. R. Stevens, Jr., B. Goplen, J. Stovall, "Beam Transport Studies on the Proton Beam Line in the Injector Complex of LAMPF," Proc. this Conference.

385

graph of one of the viewing screen devices is shown in Fig. 11, and the beam cross sections now obtained along the beam line are shown in Fig. 12.

Work is now in progress to eliminate the halo structures present in these beams. Prototype beam scrapers have been installed and tested and high power units are now being built. The present scrapers remove ~ 6 mA of beam, primarily at the prebuncher, and result in a 28-mA beam at the linac entrance with an emittance of 1.2 π cm-mrad at 750 keV. Most of the halo structure previously present at this point has now been eliminated. The installa- of beam scrapers is expected to facilitate the tuning of the injector beam line as well as reducing beam loss in the linac.
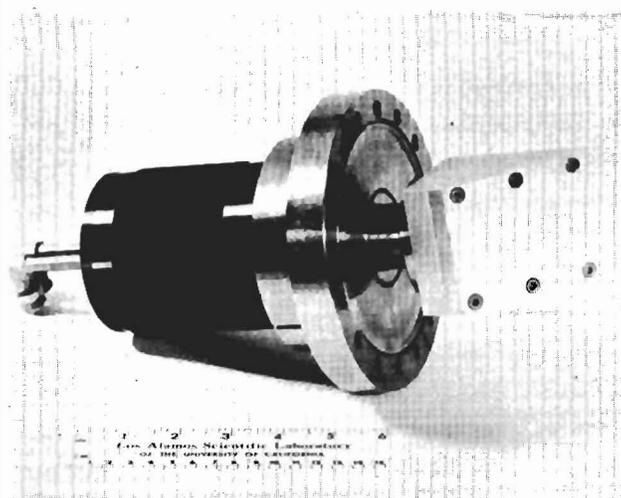

TAVSOI
43 m A

TDVSOI
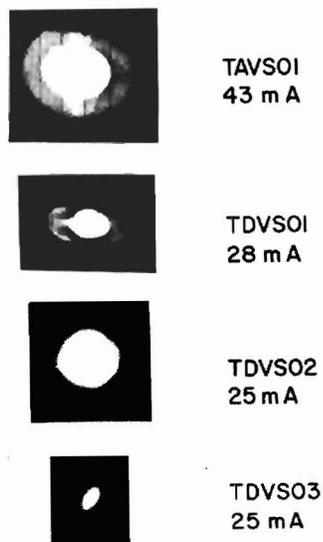28 m A

TDVSO2
25 m A

TDVSO3
25 m A

Fig. 12. Beam cross sections observed along the proton beam transport line.

REFERENCES

1. P. W. Allison, C. R. Emigh, D. W. Mueller, R. R. Stevens, Jr., "Operation of the LAMPF 750-keV Injector," Proc. 1971 Particle Accelerator Conference, NS-18, 3 (1971).

2. J. H. Singleton, "Hydrogen Pumping Speed of Sputter-Ion Pumps," J. of Vac. Sci., 6, 316 (Mar/April 1969).

3. J. H. Singleton, "Hydrogen Pumping by Sputter-Ion Pumps and Getter Pumps," J. For Vac. Sci. Technol. 8, 275 (Jan/Feb 1971).

4. S. L. Rutherford and R. L. Papsen, "Enhanced Hydrogen Pumping with Sputter-Ion Pumps," Rev. Sci. Instr. 32, 1144 (1961).

5. P. W. Allison, C. R. Emigh, and R. R. Stevens, Jr., "Initial Operation of the Beam-Transport System in the LAMPF Injector Complex," Proc. of the 1970 Proton Linear Accelerator Conference, Pt. 1, pp. 143-149 (1970).

Fig. 11. Beam viewing screen device.